Infinite Elements for the Analysis of Open Dielectric Waveguides

MARC J. McDOUGALL AND J. P. WEBB, MEMBER, IEEE

Abstract—**The finite element method is applied to the modal analysis of unbounded, arbitrarily shaped, and arbitrarily inhomogeneous dielectric waveguides with the use of new infinite elements incorporating several radially decaying exponential trial functions. The outer optimization loop required by previous methods employing a single decaying trial function is eliminated and all modes corresponding to a given phase constant are calculated in one pass of the solver. The method is tested with examples of slab, circular, and square dielectric waveguides.**

I. Introduction

VARIOUS USEFUL unbounded dielectric waveguide structures (e.g. optical fibers, planar diffused guides) have been proposed or fabricated which have irregular shapes or permittivity distributions. The modal fields of these guides are described by the vector Helmholtz equation. Finding a closed-form analytical expression for the modes of these unbounded guides is usually impossible unless the waveguide geometry and the permittivity profile are identical with the coordinate curves of a coordinate system in which the Helmholtz equation is separable. The application of a numerical method is the only recourse for solving the general dielectric waveguide problem.

A new infinite element is presented for the modal analysis of a general class of unbounded translationally symmetric dielectric waveguides. This class includes unbounded dielectric guides with arbitrarily shaped cross sections and arbitrarily inhomogeneous permittivity profiles. It is applied here to sourceless, lossless, isotropic guides with uniform permeability $\mu = \mu_0$. For brevity, members of this class shall be referred to simply as *open guides.*

II. The FEM and the Unbounded Vector Helmholtz Eigenproblem

In the following, a field time dependence of $e^{j\omega t}$ is assumed and c is the speed of light in vacuo. In terms of the magnetic field intensity phasor $\boldsymbol{H}(x, y, z)$, the relative permitivity ϵ_r, and the wavenumber $k_0 = \omega/c$, the vector Helmholtz equation is

$$\nabla \times \left(\frac{1}{\epsilon_r} \nabla \times \boldsymbol{H} \right) - k_0^2 \boldsymbol{H} = \boldsymbol{0}. \tag{1}$$

Of the numerous numerical techniques that have been proposed for the analysis of closed dielectric guides, the finite element method (FEM) has achieved wide acceptance because of its ability to accommodate inhomogeneous materials [1]–[3]. Another advantage of the FEM is that it reduces algebraically to the linear eigenproblem $Aa = \lambda Ba$, for which efficient and reliable solution techniques are available. Since regular elements are of finite size and cannot be used to mesh infinite regions, the FEM must be adapted with some special technique to solve unbounded problems.

One approach is to couple the FEM to another method more suitable for an unbounded region such as function expansions [4] or integral equations [5], [6]. These techniques are used in the the exterior region, which is usually homogeneous, while the FEM is applied to an interior region which includes all inhomogeneity. Unfortunately, these hybrid methods have the disadvantage of removing the linearity of the algebraic problem. Instead of solving a generalized eigenvalue problem, the solutions must be found by a costly search for the roots of a determinant and the solutions must then be verified carefully to ensure that no roots are omitted. To date, no one has described a hybrid method based on the three-component $\boldsymbol{H}$ formulation [7], [8] which preserves linearity.

To preserve the linearity of the FEM, the following methods have been proposed. The virtual boundary technique [9] consists of enclosing the open guide in a conducting box whose dimensions are large in comparison to the size of the core region and meshing the entire problem with finite elements. The drawback is that, for a given accuracy, the correct location of the virtual boundary is unknown, although it can be determined iteratively [10]. Also, the exterior mesh must be made very large near cutoff, which results in a very large algebraic problem to solve. The conformal mapping method of Wu and Chen [11] can only be applied to open guides having a plane of symmetry. The ballooning method employs a recursive meshing technique for the exterior region, but this method

Manuscript received December 15, 1988; revised June 12, 1989. This work was supported by the Natural Sciences and Engineering Research Council of Canada and the Centre de Recherches en Informatique de Montréal.

M. J. McDougall was with the Department of Electrical Engineering, McGill University, Montreal, Canada. He is now with MPB Technologie Inc., Dorval, Que., Canada.

J. P. Webb is with the Department of Electrical Engineering, McGill University, Montréal, Canada H3A 2A7.

IEEE Log Number 8930658.

0018-9480/89/1100-1724$01.00 ©1989 IEEE

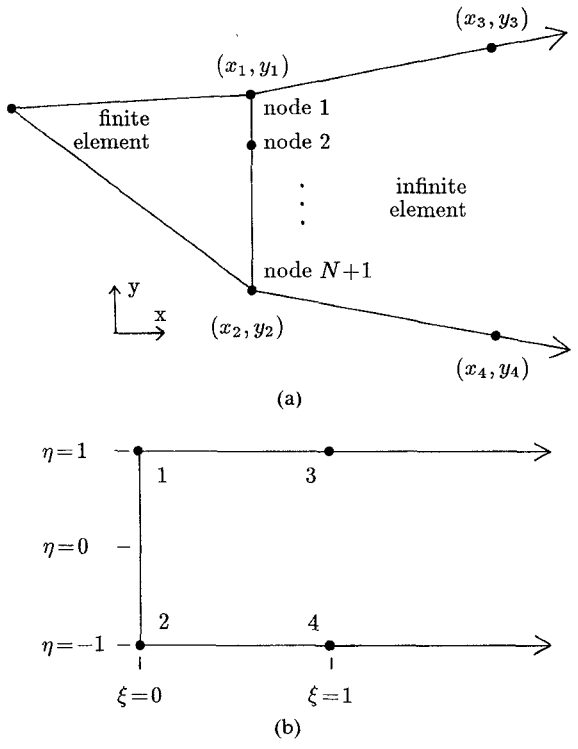

Fig. 1. The infinite element in (a) the $x-y$ plane and (b) the $\xi-\eta$ plane.

seems to be applicable only to the Laplace problem [12], [13] and the scalar Helmholtz eigenproblem [14].

In the method of infinite elements, the interior region is meshed with finite elements while the exterior is meshed with elements having infinite area. A discussion of this method follows.

III. Infinite Elements for Open Guides

Many infinite elements have been proposed [15]–[18] for solving deterministic (i.e., noneigenvalue) unbounded problems such as the Laplace equation. For these problems, the asymptotic behaviour of the solution is in general known in advance and an approximately correct decaying trial function can be defined inside each infinite element. In the case of the vector Helmholtz equation, however, the selection of trial functions is much more difficult since the asymptotic behavior is different for each mode and varies with the frequency.

For the analysis of open guides, Yeh *et al.* [19] used the FEM with parametric infinite elements which incorporated a radial trial function of the form $\gamma = e^{-\alpha r}$ where $\alpha > 0$. The asymptotic field behavior is therefore specified by the decay length $1/\alpha$, which is globally defined for the whole problem. Because at the outset the correct decay is unknown, an outer iteration loop was added to the FEM which optimized the α parameter for each mode of interest.

Rahman and Davies [20] employed similar elements whose decay was specified in the x direction by e^{-x/L_x} or in the y direction by e^{-y/L_y} or in both by $e^{-x/L_x - y/L_y}$. The decay lengths were optimized in an outer iteration loop, as with Yeh *et al.* Methods such as these which employ infinite elements incorporating an optimized single exponential decay per coordinate in each element will be referred to as *optimized single decay* (OSD) methods. Although it was formulated for the scalar Helmholtz problem, the two techniques proposed by Hayata *et al.* [21] are also OSD methods which iterate to the optimal exponential decay parameter efficiently by using either the previous eigenvectors or the previous eigenvalue to calculate the next estimate of the decay length.

The infinite element method presented here makes the above decay length optimization unnecessary and conserves the linearity of the FEM. The interior region of the guide, which contains all inhomogeneity, is meshed with triangular finite elements [22] and the exterior of the guide is meshed with infinite elements whose shape results from the mapping of a semi-infinite strip in the $\xi-\eta$ into the $x-y$ plane (see Fig. 1) using the following mapping function:

$$\begin{aligned} x = {} & x_1\left(\frac{1+\eta}{2}\right)(1-\xi) & y = {} & y_1\left(\frac{1+\eta}{2}\right)(1-\xi) \\ & + x_2\left(\frac{1-\eta}{2}\right)(1-\xi) & & + y_2\left(\frac{1-\eta}{2}\right)(1-\xi) \\ & + x_3\left(\frac{1+\eta}{2}\right)\xi & & + y_3\left(\frac{1+\eta}{2}\right)\xi \\ & + x_4\left(\frac{1-\eta}{2}\right)\xi & & + y_4\left(\frac{1-\eta}{2}\right)\xi \end{aligned} \tag{2}$$

The trial functions defined in the finite elements are polynomials of order N which are interpolatory at $N_0 = (N+1)(N+2)/2$ regularly spaced nodes. Each infinite element is adjacent to a finite element, as shown in Fig. 1(a), and has $N+1$ nodes along their shared edge. The infinite element trial functions are defined in terms of the (ξ, η) variables as follows:

$$\mathbf{H}(\eta, \xi) = \sum_{u=1}^{N+1} \psi_u(\eta)\left(\gamma_{ux}\boldsymbol{i} + \gamma_{uy}\boldsymbol{j} - j\gamma_{uz}\boldsymbol{k}\right) \tag{3}$$

where the $\psi_u(\eta)$ and $(\gamma_{ux}(\xi), \gamma_{uy}(\xi), \gamma_{uz}(\xi))$ functions represent the azimuthal and radial dependences respectively of the trial function associated with node u. An axial dependence of $e^{-j\beta z}$ is assumed, where β is the phase constant; therefore the magnetic field phasor is given by $\boldsymbol{H} = \mathbf{H}e^{-j\beta z}$. For continuity of the fields across the edge shared with the triangular element, the $\psi_u(\eta)$ are defined in manner similar to the triangular element trial functions:

$$\begin{aligned} \psi_u(\eta) &= P_{u-1}\left(\frac{1+\eta}{2}\right) P_{N+1-u}\left(\frac{1-\eta}{2}\right) \\ &= \sum_{k=0}^{N} C_{uk}\eta^k \end{aligned} \tag{4}$$

where

$$P_d(\nu) = \begin{cases} \prod_{q=1}^{d} \left(\dfrac{N\nu - q + 1}{q} \right) & \text{if } d \geq 1 \\ 1 & \text{if } d = 0. \end{cases} \quad (5)$$

The $(\gamma_{ux}(\xi), \gamma_{uy}(\xi), \gamma_{uz}(\xi))$ functions consist of linear combinations of exponential decays with weights $(a_{umx}, a_{umy}, a_{umz})$ where $(1 \leq u \leq N+1;\ 0 \leq m \leq q-1)$:

$$\gamma_{ux} = a_{u0x} e^{-\xi/L_0} + \sum_{m=1}^{q-1} a_{umx} (e^{-\xi/L_m} - e^{-\xi/L_0})$$

$$\gamma_{uy} = a_{u0y} e^{-\xi/L_0} + \sum_{m=1}^{q-1} a_{umy} (e^{-\xi/L_m} - e^{-\xi/L_0})$$

$$\gamma_{uz} = a_{u0z} e^{-\xi/L_0} + \sum_{m=1}^{q-1} a_{umz} (e^{-\xi/L_m} - e^{-\xi/L_0}). \quad (6)$$

The decay lengths $(L_0, L_1, \cdots, L_{q-1})$ are selected to specify a range of decays that will allow the $(\gamma_{ux}(\xi), \gamma_{uy}(\xi), \gamma_{uz}(\xi))$ trial function to adequately model the asymptotic behavior of all modes of interest simultaneously. These decay lengths are not optimized, so the method is called the multiple fixed decay (MFD) method. The addition of the unknown variables $(a_{umx}, a_{umy}, a_{umz};\ 1 \leq u \leq N+1;\ 1 \leq m \leq q-1)$ does increase the problem size relative to the OSD method and therefore also increases the execution time of the eigenvalue solver, but this is offset by the removal of the outer optimization loop and by the fact that all p modes are found in one execution of the solver.

IV. Implementation

In the following, the symbol Ω represents the cross section of the open guide which is in the $x-y$ plane (the z axis is the axis of the guide). The perfect electric and magnetic boundary contours are represented by the notation $\partial\Omega_s$ and $\partial\Omega_o$, respectively. The FEM formulation uses Berk's functional [7] with an added penalty term for the elimination of spurious modes [8], [23]–[25]:

$$k_0^2(\boldsymbol{H}) = \frac{\int_\Omega (\nabla \times \boldsymbol{H})^* \cdot \dfrac{1}{\epsilon_r} (\nabla \times \boldsymbol{H}) + \dfrac{1}{\epsilon_{r\min}} (\nabla \cdot \boldsymbol{H})^* (\nabla \cdot \boldsymbol{H})\, dx\, dy}{\int_\Omega \boldsymbol{H}^* \cdot \boldsymbol{H}\, dx\, dy} \quad (7)$$

where k_0 is the wavenumber and $\epsilon_{r\min}$ is the minimum relative permittivity. The essential conductor and far-field boundary conditions are

$$\boldsymbol{H} \times \boldsymbol{n} = \boldsymbol{0} \quad \text{on } \partial\Omega_0 \quad (8)$$

$$\boldsymbol{H} \cdot \boldsymbol{n} = 0 \quad \text{on } \partial\Omega_s \quad (9)$$

$$\lim_{r \to \infty} \sqrt{r}\, \boldsymbol{H} = \boldsymbol{0} \quad (10)$$

$$\lim_{r \to \infty} \sqrt{r}\, \nabla \times \boldsymbol{H} = \boldsymbol{0} \quad (11)$$

$$\lim_{r \to \infty} \sqrt{r}\, \nabla \cdot \boldsymbol{H} = 0 \quad (12)$$

where $r = \sqrt{x^2 + y^2}$. The boundary conditions (10), (11), and (12) are far-field boundary conditions [25]. The FEM consists in inserting the trial functions of the meshed problem region into the functional; the eigenvalues are then obtained by taking the first variation of the functional and solving the resulting generalized eigenvalue equation.

The substitution and integration of triangular element trial functions and the subsequent application of boundary conditions are well documented elsewhere [22], [23]. The expressions that result when the infinite element trial functions are substituted into (7) are given in the Appendix. When expanded, both the numerator and the denominator consist of sums of integrals of the following form:

$$I_{a,b,c}(L) = \int_{-1}^{1} \int_{0}^{\infty} e^{-\xi/L} \xi^a \eta^b J^c\, d\xi\, d\eta \quad (13)$$

where

$$a = 0, 1, 2$$

$$b = 0, 1, \cdots, (2N+2)$$

$$c = -1, 0, 1$$

and J is the Jacobian of the mapping from the (x, y) to the (ξ, η) domain:

$$J = \left| \frac{\partial(x, y)}{\partial(\xi, \eta)} \right| = J_1 + J_2 \xi + J_3 \eta. \quad (14)$$

Numerical integration is not employed to evaluate these integrals since no Gauss cubature rule with error bounds exists for this integral, which makes the number of Gauss points required uncertain. Instead, the integrals are calculated using a semiclosed formula [26, p. 321]. In order to simplify the code, all the infinite elements are shaped in a way that makes J_3 in (14) vanish. All infinite element shapes whose Jacobian satisfies $J_3 = 0$ are symmetric about the line $\eta = 0$ in the $x-y$ plane (see Fig. 2(b)). This is not restrictive since the region occupied by any infinite element can be meshed by a symmetric infinite element in combination with triangular finite elements (see the example in Fig. 2). The problem size is increased slightly by the addition of the finite elements but this simplifies immensely the code required to integrate the infinite elements.

A Fortran program called OMAX was written to implement the MFD method. The program accepts as input a data file which describes the problem mesh, the material permittivities, the boundary conditions, and the desired phase constants β. For each β, it assembles the global matrices, solves the generalized eigenvalue problem, and outputs a list of the lowest p eigenvalues.

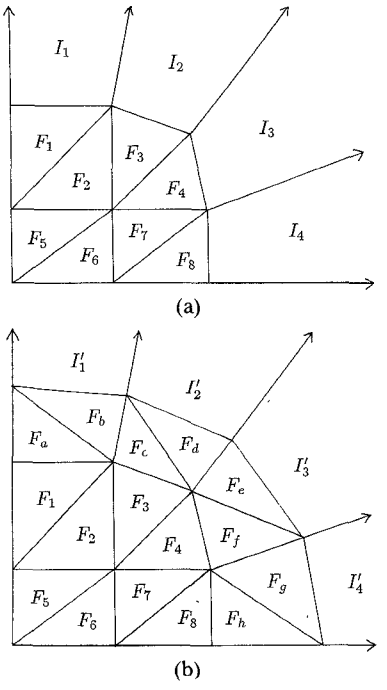

Fig. 2. The asymmetrical infinite elements $I_1 - I_4$ in (a) are converted to symmetrical infinite elements $I'_1 - I'_4$ in (b) with the addition of finite elements $F_a - F_h$.

V. The Selection of Decay Lengths

The q fixed decay lengths $(L_0, L_1, \cdots, L_{q-1})$ that are supplied to the trial functions of each infinite element are selected automatically by the OMAX program. In the examples, q is set to either 5 or 6 with good results. Increasing q causes more radial trial functions to be allocated to each infinite element, which tends to reduce the error in the results but also increases the computation time.

The decay length selection algorithm starts by calculating an estimate $L_{\min}$ of the shortest decay length required to model any mode for a particular choice of the phase constant β. Let $\epsilon_{r\max}$ and $\epsilon_{r\min}$ be the maximum relative permittivity of the problem (usually located in the core) and the minimum relative permittivity (usually in the infinite region) respectively. Now for an open guide consisting simply of a circular homogeneous core (of any radius) of relative permittivity $\epsilon_{r\max}$ surrounded by a cladding of relative permittivity $\epsilon_{r\min}$, the following relation holds [27, p. 367]:

$$[\max(h)]^2 = (\epsilon_{r\max} - \epsilon_{r\min}) k_0^2 \tag{15}$$

where $h = \sqrt{\beta^2 - \epsilon_r k_0^2}$ is the transverse wavenumber in the cladding. Putting this in terms of $\max(h)$ and β only,

$$[\max(h)]^2 = \left(1 - \frac{\epsilon_{r\min}}{\epsilon_{r\max}}\right)\beta^2. \tag{16}$$

The asymptotic radial behavior of the fields for this guide is $e^{-hr}/\sqrt{hr}$ [28, p. 297], and therefore an estimate

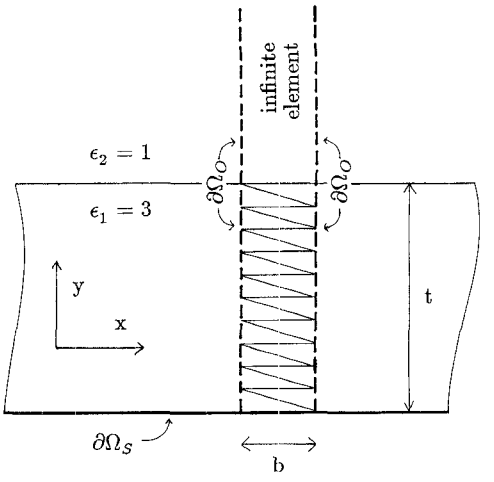

Fig. 3. The slab waveguide example with added magnetic walls.

$L_{\min}$ of the shortest decay length is

$$L_{\min} = \frac{1}{\max(h)} = \frac{1}{\left(1 - \frac{\epsilon_{r\min}}{\epsilon_{r\max}}\right)^{1/2}\beta}. \tag{17}$$

Starting with this estimate, the decay lengths are generated by repeated multiplication by the coefficient C_d:

$$L_{i+1} = C_d L_i. \tag{18}$$

The user-selected parameter C_d therefore controls the distribution of the decay lengths. For all the test examples, it is set to the value 10. This value causes OMAX to specify decay lengths which are very large relative to the core dimensions of the guides, and thus permits the modeling of the modes very near to cutoff.

Since the fields may have features which are small in comparison to $\max(h)$, the user can specify a number N_{nf} of *near-field* decay lengths. These are also generated from $L_{\min}$ by successive division by C_d. In summary, all decay lengths are generated by the formula

$$L_i = L_{\min}(C_d)^{i - N_{\text{nf}}}, \qquad i = 0, 1, \cdots, (q-1). \tag{19}$$

Most of the computation time is spent assembling the infinite element global matrix contribution and solving the generalized eigenvalue problem. Although the global matrices are sparse and a solver which made use of sparsity would be more efficient, a dense matrix solver was used for the tests below. The solver is composed of EISPACK routines [29] which convert the generalized eigenvalue problem to a standard eigenvalue problem, tridiagonalize the resulting matrix, and then use Sturm sequencing to locate the eigenvalues.

VI. Examples

A. The Slab Waveguide

As a simple example and test of the MFD technique, consider the problem of determining the TM modes with no x variation of the slab waveguide shown in Fig. 3. The guide consists of a homogeneous dielectric film with relative permittivity $\epsilon_{r1} = 3$ and thickness t, deposited on a

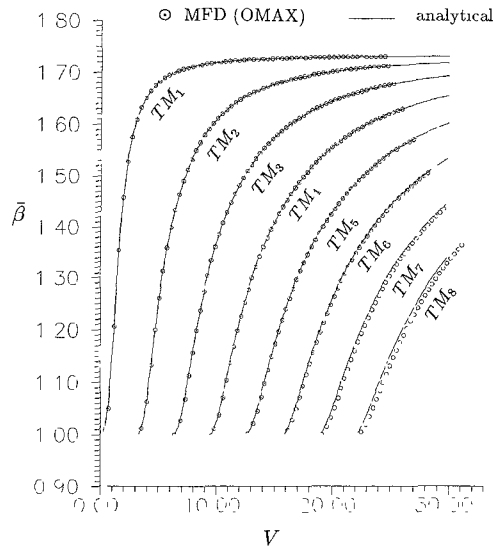

Fig. 4. The slab waveguide results using the mesh of Fig. 3, second-order triangles, $\epsilon_{r1}=3.0$, $\epsilon_{r2}=1.0$, $q=6$, $C_d=10.0$, $N_{\mathrm{nf}}=2$, $s=1.0$, $\bar{\beta}=\beta/k_0$, $V=tk_0\sqrt{\epsilon_{r1}-\epsilon_{r2}}$, and $b=t/10$.

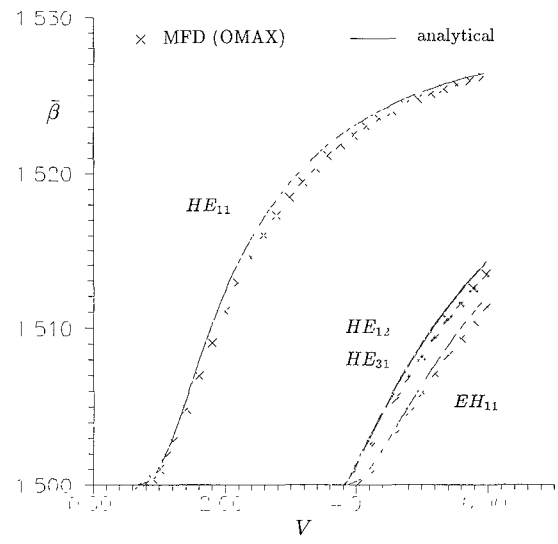

Fig. 6. The circular dielectric waveguide results using the mesh of Fig. 5, third-order triangles, $n_1=\sqrt{\epsilon_{r1}}=1.53$, $n_2=\sqrt{\epsilon_{r2}}=1.50$, $q=5$, $C_d=10.0$, $N_{\mathrm{nf}}=2$, $s=1.0$. $\bar{\beta}=\beta/k_0$, and $V=ak_0\sqrt{\epsilon_{r1}-\epsilon_{r2}}$.

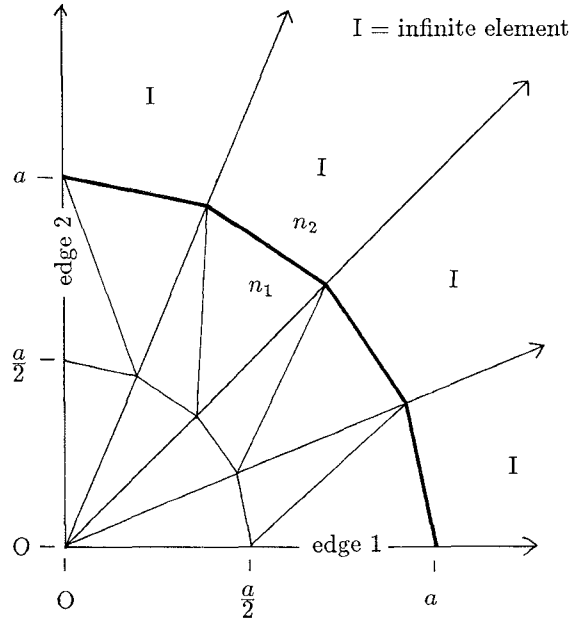

Fig. 5. The circular dielectric waveguide example.

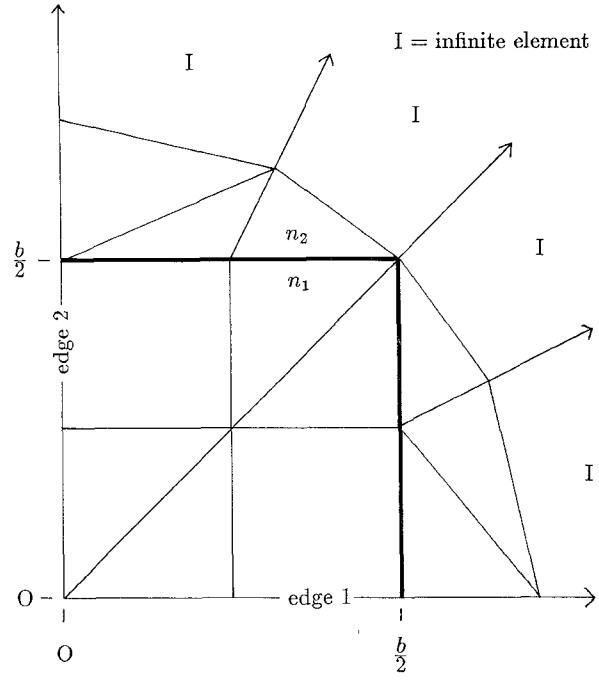

Fig. 7. The square dielectric waveguide example.

conducting plane located at $y=0$. The surrounding homogeneous cladding has relative permittivity $\epsilon_{r2}=1$. The desired modes can be found by adding two perfect magnetic boundary walls and meshing the region between them (see Fig. 3). If the distance b between the magnetic walls is set to a value small relative the the film thickness t, then the lowest modes are those with no x variation.

The results from the OMAX program with second-order triangles and six decays are shown in Fig. 4; the normalised $\bar{\beta}$ versus V coordinates are used. The analytical solutions are shown as the solid lines. Very close agreement is obtained for the lowest modes from cutoff to the highest frequencies shown on the graph.

B. The Circular Dielectric Waveguide

The next example is the weakly guiding circular waveguide with interior and exterior refractive indices of $n_1=\sqrt{\epsilon_{r1}}=1.53$ and $n_2=\sqrt{\epsilon_{r2}}=1.50$, respectively, and radius a. Closed-form analytical solutions to the modes of this guide, designated TM_{0u}, TE_{0u}, EH_{vu}, and HE_{vu} (where $u, v=1,2,\ldots$) are known [30, p. 225]. To reduce the problem size, only one quarter of the problem is meshed as shown in Fig. 5; the mesh is composed of 12 triangular and four infinite elements. The modes that result from the imposition of magnetic conductor boundaries on edges 1 and 2 respectively are shown in Fig. 6; both the OMAX and the analytical results are given. The results are most

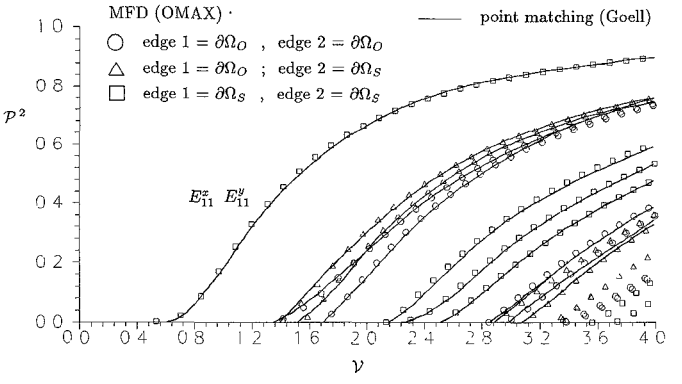

Fig. 8. The square waveguide results using the mesh of Fig. 7, second-order triangles, $n_1=\sqrt{\epsilon_{r1}}=1.50$, $n_2=\sqrt{\epsilon_{r2}}=1.00$, $q=5$, $C_d=10.0$, $N_{nf}=2$, $s=1.0$, $\mathcal{V}=(k_0 b/\pi)\sqrt{\epsilon_{r1}/\epsilon_{r2}-1}$ and $\mathcal{P}^2=[(\beta/k_0)^2-1]/[(\epsilon_{r1}/\epsilon_{r2})-1]$.

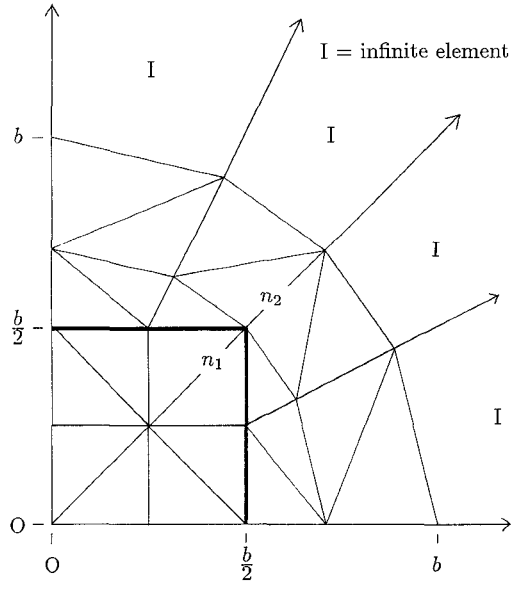

Fig. 9. The mesh used for the OSD method results shown in Fig. 10.

accurate at cutoff and toward the higher frequencies, and the maximum error in k_0 for all the modes shown is 0.03 percent. The global matrix order was 325.

C. The Square Dielectric Waveguide

Using point-matching, Goell [31] calculated the dispersion curves of the modes of the square dielectric waveguide for which no exact analytical solutions are available. As with the circular waveguide, a quarter mesh was used (Fig. 7) and three distinct pairs of edge 1 and 2 boundary conditions were applied separately. In Fig. 8 the OMAX results compare well with the point matching results.

With the boundary conditions on edges 1 and 2 both set to $\partial\Omega_o$, the execution time for each β value was 12 minutes on a VAX 8650 and the order of the global matrices was 338.

D. A Comparison of the MFD and OSD Techniques

The drawback of the OSD method is that the single decay length L must be optimized, particularly near cutoff. This is illustrated in Fig. 10. Each solid line is a plot of the normalized frequency bk_0 of the fundamental mode versus b/L, for one particular value of $b\beta$, computed by the OSD method using the mesh of Fig. 9. There are 12 such lines, for $b\beta$ values ranging from 1 to 3.75. The need for optimization with the OSD technique is made apparent by the severe variation of the frequencies with decay length.

The results of the MFD method applied to the mesh of Fig. 7 are included for comparison (they are horizontal since they do not vary with b/L). Although the mesh is smaller, the results of the MFD technique compare very well with the optimum OSD results.

VII. Conclusions

In extending the FEM to accommodate open guides through the use of infinite elements, the need to optimize the decay lengths for each mode is eliminated by incorporating several fixed decay trial functions into each infinite element. The first p modes can be calculated in just one pass of the solver.

Appendix

The contributions to the global matrix from an infinite element can be calculated by first decomposing the functional (7) into three integrals:

$$I_1(\boldsymbol{H})=\int_\Omega(\nabla\times\boldsymbol{H})^*\cdot\frac{1}{\epsilon_r}(\nabla\times\boldsymbol{H})\,dx\,dy$$

$$I_2(\boldsymbol{H})=\int_\Omega(\nabla\cdot\boldsymbol{H})^*(\nabla\cdot\boldsymbol{H})\,dx\,dy$$

$$I_3(\boldsymbol{H})=\int_\Omega\boldsymbol{H}^*\cdot\boldsymbol{H}\,dx\,dy. \tag{20}$$

The contributions to each integral corresponding to each pair of unknown weight vectors $(a_{umx}, a_{umy}, a_{umz})$ and $(a_{u'm'x}, a_{u'm'y}, a_{u'm'z})$ (see (6)) are then given by Tables I, II, and III. In these tables,

$$\begin{aligned}U_{ump,u'm'p'}&=\mathcal{U}_{ump,u'm'p'}-\delta_{m'0}\mathcal{U}_{ump,u'0p'}\\&\quad-\delta_{m0}\mathcal{U}_{u0p,u'm'p'}+\delta_{m0}\delta_{m'0}\mathcal{U}_{u0p,u'0p'}\\V_{ump,u'm'}&=\mathcal{V}_{ump,u'm'}-\delta_{m'0}\mathcal{V}_{ump,u'0}\\&\quad-\delta_{m0}\mathcal{V}_{u0p,u'm'}+\delta_{m0}\delta_{m'0}\mathcal{V}_{u0p,u'0}\\W_{um,u'm'}&=\mathcal{W}_{um,u'm'}-\delta_{m'0}\mathcal{W}_{um,u'0}-\delta_{m0}\mathcal{W}_{u0,u'm'}\\&\quad+\delta_{m0}\delta_{m'0}\mathcal{W}_{u0,u'0}\\&\qquad p,p'=x\text{ or }y.\end{aligned} \tag{21}$$

In these expressions, δ_{ij} is the Kronecker delta and

$$\mathcal{U}_{ump,u'm'p'},\ \mathcal{V}_{ump,u'm'},$$

and

$$\mathcal{W}_{um,u'm'}$$

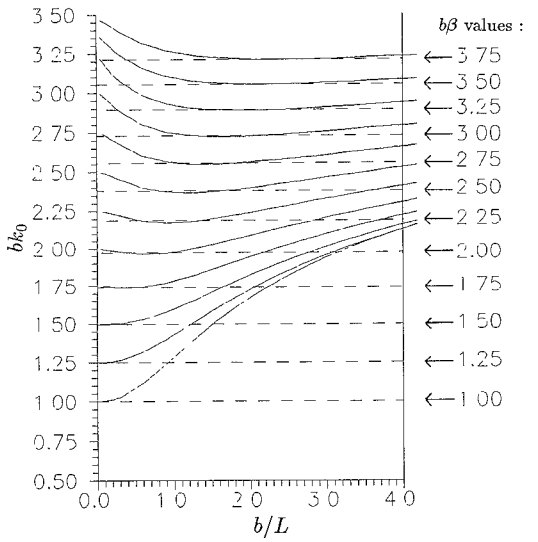

mesh of Figure 7
second order triangles
$n_1 = \sqrt{\epsilon_{r1}} = 1.50$
$n_2 = \sqrt{\epsilon_{r2}} = 1.00$
$q = 6$
$C_d = 10.0$
$N_{nf} = 2$
$s = 1.0$

mesh of Figure 9
second order triangles
$n_1 = \sqrt{\epsilon_{r1}} = 1.50$
$n_2 = \sqrt{\epsilon_{r2}} = 1.00$
$q = 1$
$s = 1.0$

Fig. 10. A comparison of the OSD and MFD techniques for the fundamental mode of the square waveguide. The solid curves illustrate the variation of bk_0 with b/L using the OSD technique for the 12 values of normalized phase constant $b\beta$ shown on the right. The dashed lines represent the results of the MFD technique with six fixed decays for the same values of $b\beta$.

TABLE I
THE CONTRIBUTION TO THE INTEGRAL I_1

	$a_{u'm'x}$	$a_{u'm'y}$	$a_{u'm'z}$
a_{umx}	$\frac{1}{\epsilon_r}(\beta^2 W_{um,u'm'} + U_{umy,u'm'y})$	$-\frac{1}{\epsilon_r} U_{umy,u'm'x}$	$-\frac{1}{\epsilon_r}\beta V_{u'm'x,um}$
a_{umy}	$-\frac{1}{\epsilon_r} U_{umx,u'm'y}$	$\frac{1}{\epsilon_r}(\beta^2 W_{um,u'm'} + U_{umx,u'm'x})$	$-\frac{1}{\epsilon_r}\beta V_{u'm'y,um}$
a_{umz}	$-\frac{1}{\epsilon_r}\beta V_{umx,u'm'}$	$-\frac{1}{\epsilon_r}\beta V_{umy,u'm'}$	$\frac{1}{\epsilon_r}(U_{umy,u'm'y} + U_{umx,u'm'x})$

TABLE II
THE CONTRIBUTION TO THE INTEGRAL I_2

	$a_{u'm'x}$	$a_{u'm'y}$	$a_{u'm'z}$
a_{umx}	$U_{umx,u'm'x}$	$U_{umx,u'm'y}$	$-\beta V_{umx,u'm'}$
a_{umy}	$U_{umy,u'm'x}$	$U_{umy,u'm'y}$	$-\beta V_{umy,u'm'}$
a_{umz}	$-\beta V_{u'm'x,um}$	$-\beta V_{u'm'y,um}$	$\beta^2 W_{um,u'm'}$

TABLE III
THE CONTRIBUTION TO THE INTEGRAL I_3

	$a_{u'm'x}$	$a_{u'm'y}$	$a_{u'm'z}$
a_{umx}	$W_{um,u'm'}$	0	0
a_{umy}	0	$W_{um,u'm'}$	0
a_{umz}	0	0	$W_{um,u'm'}$

TABLE IV
THE C_{uk} COEFFICIENTS

		$k=0$	$k=1$	$k=2$	$k=3$	$k=4$
1st order (N=1)	$u=1$	1/2	1/2	—	—	—
	$u=2$	1/2	-1/2	—	—	—
2nd order (N=2)	$u=1$	0	1/2	1/2	—	—
	$u=2$	1	0	-1	—	—
	$u=3$	0	-1/2	1/2	—	—
3rd order (N=3)	$u=1$	-1/16	-1/16	9/16	9/16	—
	$u=2$	9/16	27/16	-9/16	-27/16	—
	$u=3$	9/16	-27/16	-9/16	27/16	—
	$u=4$	-1/16	1/16	9/16	-9/16	—
4th order (N=4)	$u=1$	0	-1/6	-1/6	2/3	2/3
	$u=2$	0	4/3	8/3	-4/3	-8/3
	$u=3$	1	0	-5	0	4
	$u=4$	0	-4/3	8/3	4/3	-8/3
	$u=5$	0	1/6	-1/6	-2/3	2/3

TABLE V
THE a_{pi} COEFFICIENTS

	$i=0$	$i=1$
$p=x$	$\frac{1}{2}(y_1 - y_2)$	$\frac{1}{2}(-y_1 + y_2 + y_3 - y_4)$
$p=y$	$\frac{1}{2}(-x_1 + x_2)$	$\frac{1}{2}(x_1 - x_2 - x_3 + x_4)$

TABLE VI
THE b_{pi} COEFFICIENTS

	$i=0$	$i=1$
$p=x$	$\frac{1}{2}(y_1 + y_2 - y_3 - y_4)$	$\frac{1}{2}(y_1 - y_2 - y_3 + y_4)$
$p=y$	$\frac{1}{2}(-x_1 - x_2 + x_3 + x_4)$	$\frac{1}{2}(-x_1 + x_2 + x_3 - x_4)$

are given by

$$\begin{aligned}\mathcal{U}_{ump,u'm'p'} = \sum_{k,l=0}^{N} C_{uk}C_{vl} \sum_{i,j=0}^{1} \Big[& klb_{pi}b_{p'j}I_{0,k+l+i+j-2,-1}(L) \\ & - kb_{pi}a_{p'j}I_{j,k+l+i-1,-1}(L) \\ & - la_{pi}b_{p'j}I_{i,k+l+j-1,-1}(L) \\ & + a_{pi}b_{p'j}I_{i+j,k+l,-1}(L)\Big] \\ \mathcal{V}_{ump,u'm'} = \sum_{k,l=0}^{N} C_{uk}C_{vl} \sum_{i=0}^{1} \Big[& kb_{pi}I_{0,k+l+i-1,0}(L) \\ & - a_{pi}I_{0,k+l+i,0}(L)\Big] \\ \mathcal{W}_{um,u'm'} = \sum_{k,l=0}^{N} & C_{uk}C_{vl}I_{0,k+l,1}(L). \end{aligned} \tag{22}$$

In these, the integral I is given by (13) and

$$L = \left(\frac{1}{L_m} + \frac{1}{L_{m'}}\right)^{-1}. \tag{23}$$

The C_{uk} for orders 1 to 4, which are the polynomial coefficients in (4), and the a_{pi} and b_{pi} coefficients are given by Tables IV, V, and VI.

Lastly, the Jacobian coefficients J_1, J_2 and J_3 in (14) are expressed in terms of the a_{pi} and b_{pi} as

$$J_1 = b_{y0}a_{x0} - b_{x0}a_{y0}$$

$$J_2 = b_{y0}a_{x1} - b_{x0}a_{y1}$$

$$J_3 = -a_{y1}a_{x0} + a_{x1}a_{y0}. \tag{24}$$

REFERENCES

[1] M. Hano, "Finite-element analysis of dielectric-loaded waveguides," *IEEE Trans. Microwave Theory Tech.*, vol. MTT-32, pp. 1275–1279, Oct. 1984.

[2] P. Daly, "Hybrid-mode analysis of microstrip by finite-element methods," *IEEE Trans. Microwave Theory Tech.*, vol. MTT-19, pp. 19–25, Jan. 1971.

[3] Z. J. Csendes and P. Silvester, "Numerical solution of dielectric loaded waveguides: I—Finite-element analysis," *IEEE Trans. Microwave Theory Tech.*, vol. MTT-18, pp. 1124–1131, Dec. 1970.

[4] K. Oyamada and T. Okoshi, "Two-dimensional finite-element method of propagation characteristics of axially nonsymmetrical optical fibers," *Radio Sci.*, vol. 17, no. 1, pp. 109–116, Jan.–Feb. 1982.

[5] C. C. Su, "A combined method for dielectric waveguides using the finite-element technique and the surface integral equations method," *IEEE Trans. Microwave Theory Tech.*, vol. MTT-34, pp. 1440–1446, Nov. 1986.

[6] C. G. Williams and G. K. Cambrell, "Numerical solution of surface waveguide modes using transverse field components," *IEEE Trans. Microwave Theory Tech.*, vol. MTT-22, pp. 329–330, Mar. 1974.

[7] A. D. Berk, "Variational principles for electromagnetic resonators and waveguides," *IRE Trans. Antennas Propagat.*, vol. AP-4, pp. 104–111, Apr. 1956.

[8] B. M. A. Rahman and J. B. Davies, "Penalty function improvement of waveguide solution by finite elements," *IEEE Trans. Microwave Theory Tech.*, vol. MTT-32, pp. 922–928, Aug. 1984.

[9] C. Yeh, S. B. Dong, and W. Oliver, "Arbitrarily shaped inhomogeneous optical fiber or integrated opt. waveguides," *J. Appl. Phys.*, vol. 46, no. 5, May 1975.

[10] M. Ikeuchi, H. Sawami, and H. Niki, "Analysis of open-type dielectric waveguides by the finite-element iterative method," *IEEE Trans. Microwave Theory Tech.*, vol. MTT-29, pp. 234–239, Mar. 1981.

[11] R. B. Wu and C. H. Chen, "A variational analysis of dielectric waveguides by the conformal mapping technique," *IEEE Trans. Microwave Theory Tech.*, vol. MTT-33, Aug. 1985.

[12] P. Silvester, D. A. Lowther, C. J. Carpenter, and E. A. Wyatt, "Exterior finite elements for 2D field problems with open boundaries," *Proc. Inst. Elec. Eng.*, vol. 124, pp. 1267–1270, Dec. 1977.

[13] K. S. Chiang, "Finite element method for cutoff frequencies of weakly guiding fibres of arbitrary cross-section," *Opt. Quantum Electron.*, vol. 16, no. 6, pp. 487–493, Nov. 1984.

[14] K. S. Chiang, "Finite-element analysis of optical fibres with iterative treatment of the infinite 2-D space," *Opt. Quantum Electron.*, vol. 17, no. 6, pp. 381–391, 1985.

[15] O. C. Zienkiewicz, C. Emson and P. Bettess, "A novel boundary infinite element," *Int. J. Numer. Meth. Eng.*, vol. 19, pp. 393–404, 1983.

[16] P. Bettess, "More on infinite elements," *Int. J. Numer. Meth. Eng.*, vol. 15, pp. 1613–1626, 1980.

[17] G. Beer and J. L. Meek, "'Infinite domain' elements," *Int. J. Numer. Meth. Eng.*, vol. 17, pp. 43–52, 1981.

[18] O. C. Zienkiewicz, K. Bando, P. Bettess, C. Emson, and T. C. Chiam, "Mapped infinite elements for exterior wave problems," *Int. J. Numer. Method. Eng.*, vol. 21, pp. 1229–1251, 1985.

[19] C. Yeh, K. Ha, S. B. Dong, and W. P. Brown, "Single-mode optical waveguides," *Appl. Opt.*, vol. 18, no. 10, pp. 1490–1504, May 1979.

[20] B. M. A. Rahman and J. B. Davies, "Finite element analysis of optical and microwave problems," *IEEE Trans. Microwave Theory Tech.*, vol. MTT-32, pp. 20–28, Jan. 1984.

[21] K. Hayata, M. Eguchi, and M. Koshiba, "Self-consistent finite/infinite element scheme for unbounded guided wave problems," *IEEE Trans. Microwave Theory Tech.*, vol. 36, pp. 614–616, Sept. 1988.

[22] P. P. Silvester and R. L. Ferrari, *Finite Elements for Electrical Engineers*. Cambridge, England: Cambridge University Press, 1983.

[23] M. Koshiba, H. Kazuya, and M. Suzuki, "Improved finite-element formulation in terms of the magnetic field vector for dielectric waveguides," *IEEE Trans. Microwave Theory Tech.*, vol. MTT-33, pp. 227–233, Mar. 1985.

[24] J. P. Webb, "The finite element method for finding modes of dielectric-loaded cavities," *IEEE Trans. Microwave Theory Tech.*, vol. MTT-33, pp. 635–639, July 1985.

[25] M. J. McDougall, "Infinite elements for the analysis of open dielectric waveguides," M.Sc. thesis, Dept. Elec. Eng., McGill University, Montreal, 1988.

[26] I. S. Gradshteyn, and I. M. Ryzhik, *Tables of Integrals, Series, and Products*, corrected and enlarged ed. New York, Academic Press, 1980.

[27] J. D. Jackson, *Classical Electrodynamics*. New York: Wiley, 1975.

[28] D. Marcuse, *Light Transmission Optics*. New York: Van Nostrand Reinhold, 1982.

[29] B. S. Garbow, J. M. Boyle, J. J. Dongarra, C. B. Moler, *Matrix Eigensystem Routines — EISPACK Guide Extension*. Berlin, Germany: Springer-Verlag, 1977.

[30] M. J. Adams, *An Introduction to Optical Waveguides*. New York: Wiley, 1981.

[31] J. E. Goell, "A circular-harmonic computer analysis of rectangular dielectric waveguides," *Bell Syst. Tech. J.*, vol. 48, pp. 2133–2160, Sept. 1969.

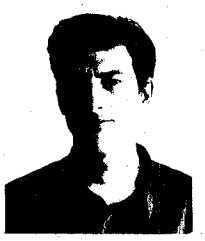

Marc J. McDougall was born in Edmonton, Alberta, Canada, on December 29, 1959. He received the B.Sc. degree in physics in 1982 and the B.Eng. and M.Eng. degrees in electrical engineering in 1985 and 1988, respectively, from McGill University, Montreal.

He is currently employed by MPB Technology Inc., Dorval, Quebec.

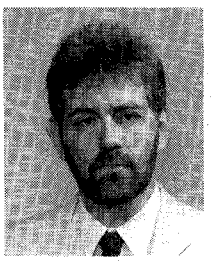

J. P. Webb (M'83) received the Ph.D. degree from Cambridge University, England, in 1981.

Since 1982 he has been an Assistant Professor, then an Associate Professor, in the Electrical Engineering Department of McGill University, Montreal, Canada. His area of research is computer methods in electromagnetics, especially the application of the finite element method.